

Development of a Passive BSAR with GNSS Transmitters of Opportunity

M. Cherniakov, R. Saini, Rui Zuo, Michael Antoniou
Electronic, Electrical and Computer Engineering
University of Birmingham, Edgbaston, Birmingham, B15 2TT

Abstract

This paper presents an overview of the research conducted at the University of Birmingham. It highlights and briefly discusses various systems parameters (e.g. resolution, power budget), problems (e.g. heterodyne channel Doppler compensation), and signal processing algorithms (imaging, synchronization) required for successfully obtaining an image.

Introduction

Synthetic aperture radar (SAR) works by collecting the echo returns from many pulses along the flight path and processing them into a single high-resolution radar image. In a monostatic SAR the transmitter and receiver are on the same platforms whereas in a bistatic SAR (BSAR) the transmitter and receiver are separated by a distance that is comparable to the expected target distance. Examples of BSAR include airborne systems where the transmitter and receiver are located on different aircrafts [1], [2]. In a space-borne system the transmitter and receiver are based on two or more satellites [3]. There is another subclass of bistatic SAR known as: space-surface bistatic synthetic aperture radar (SS-BSAR). The SS-BSAR consists of a spaceborne transmitter and a receiver, mounted on or near the earth's surface, see Figure 1. The receiver could be airborne, mounted on a ground vehicle, onboard a ship, or even in a stationary position on the ground.

The University of Birmingham (UoB) has been carrying out active research in the area of SS-BSAR since 2003. The main aim of this research is to experimentally demonstrate the feasibility and performance of airborne SS-BSAR, utilising Global Navigation Satellite System (GNSS) as the

transmitter of opportunity. This paper highlights and briefly discusses various systems parameters (resolution, power budget), problems (e.g. synchronization, Doppler compensation), and signal processing algorithms required for successfully obtaining an image.



Figure 1: SS-BSAR topology

Resolution

The GLONASS satellite was selected as the transmitter of opportunity for experimentation, despite its rather poor potential slant range resolution (30m). This was due to the fact that it was the only one available at the time of experimentation. Another GNSS system (GPS) has a navigation signal with twice the spectral width, and hence 15m potential range resolution. The most promising GNSS for the considered purposes are the EU Galileo system and the new modernized GPS signals. Figure 2 shows the signal spectrum of Galileo E5 signal. Two signal

components (E5a and E5b) in the E5 band are modulated as a single wideband signal generated following the AltBOC (15, 10) modulation. This wideband signal is centred at the frequency of 1191.795MHz and has a bandwidth of at least 50MHz. Since the E5a and E5b signals transmit independent information from each other, it's possible in theory to develop a signal processing technique that combines the received E5a and E5b signal in such a way to give a resolution of 3-8m. Similarly the different signals (P-code/M-code) of the modernized GPS L1/L2 channel can be combined to achieve 20-30MHz bandwidth or 5-8m range resolution. This makes GNSS (Galileo, GPS) based SS-BSAR a prospective candidate for many practical applications.

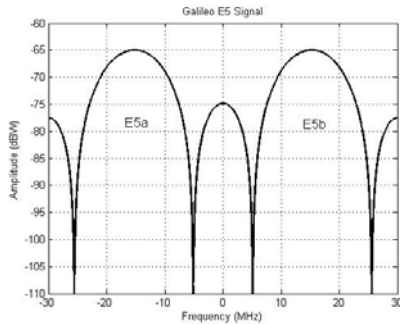


Figure 2: Galileo E5 Spectrum

Table 1 summarises some GNSS signal parameters and their potential slant range resolution. The stated resolution is for a quasi-monostatic configuration. However, for other configurations the resolution is dependent upon the geometry of the system, i.e. satellite-receiver-target positions relative to each other. The effect of the system's geometry on the resolution is comprehensively discussed in [4].

It should be noted that one of the key advantages of using a GNSS satellite compared to other satellites (e.g. Geostationary DTV satellite) is that the user can choose the desired bistatic topology (low bistatic angle, i.e. negligible resolution loss). This is due to the fact that 4 to 10 GNSS satellites are simultaneously visible at any point on the earth. As a result, a particular satellite in the best (or at least

suitable) position can be selected and there is no need for a very specific aircraft trajectory to allow the observation of an area. On the other hand geostationary satellites are fundamentally positioned above the equator and this requires a specific aircraft trajectory for mapping a particular area and, in many or even most situations, a vital loss in ground resolution may take place.

Table 1: Main parameters of GNSS signals

GNSS	GLONASS		GPS			Galileo	
	L1(P)	L2 (P)	L1(P/M)	L2 (P/M)	L5	E5a/b	E5
Channels (code)	L1(P)	L2 (P)	L1(P/M)	L2 (P/M)	L5	E5a/b	E5
Central Frequency (MHz)	1602-1615	1246-1257	1575.4	1227.6	1176	1191	1191
Minimum Power (dBW)	-161	-167	-158 (global beam) -138 (spot beam)		-154.9	-157	-154
Chip Rate (Meps)	5.11	5.11	10.23/5.11	10.23/5.11	10.23	10.23	10.23
Aggregated Bandwidth (MHz)	-	-	20-30	20-30	-	-	20-50
Range Resolution (m)	30	30	5-8	5-8	15	15	3-8

Power Budget

The receiving part of the SS-BSAR consists of two channels: the heterodyne channel is used for direct signal reception and synchronization and the radar channel is used for receiving reflected signal from the target area. The power budget of the radar channel is a determining parameter for target detection, which is calculated for the time of aperture synthesis and considering only targets that have RCS independent of frequency and angle. For bistatic SAR, the expression for SNR after range and azimuth compression can be written as [5]:

$$\frac{S}{N} = \frac{\rho A_e \sigma \lambda \eta}{4\pi R_R K T_S V_a \Delta_{az}} \quad (1)$$

where ρ is power flux density of the transmitting signal in target area, σ is the radar cross-section of the target, η is a general loss factor, R_R is the receiver-target range. Using the parameters provided in Table 1 and Equation (1), with V_a the receiver velocity 200m/s, Δ_{az} the potential azimuth resolution 1m and A_e effective area of antenna is 0.5m², Figure 3 shows the

potential target detection range for SS-B SAR using different GNSS signals. If considering 10-13 dB SNR as the radar detection threshold, targets with 50 m² RCS can be detected at the range of approximately 5 km using Galileo E5 or GPS L5 signal. By using GPS spot beam (available in 2013) the detection range can be extended to more than 50 km for target with 50 m² RCS.

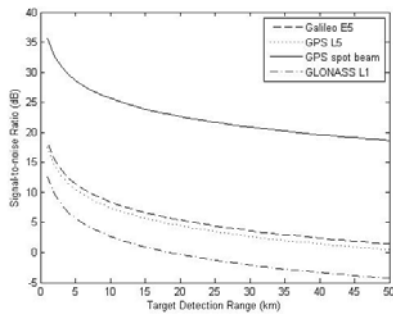


Figure 3: Detection range for 50m² RCS target

Synchronisation

Usually in a radar signal processor, the range compression consists of a correlation of the radar channel signal with the heterodyne channel signal delayed for each range resolution cell in the multi-channel correlator. In our previous publication [4] it was demonstrated that for GLONASS signal it is not possible to directly correlate the heterodyne channel with the radar channel. It needs navigation message decoding which, in turn, requires P-code synchronisation. Figure 4 shows the principles of the proposed synchronization and range compression algorithm.

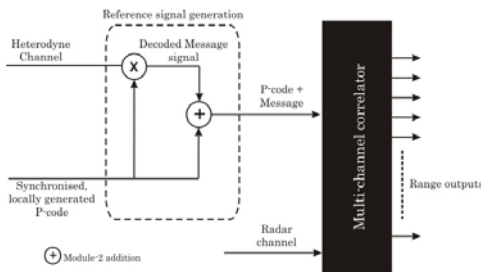


Figure 4: Range compression algorithm

The synchronisation comprises of tracking the satellite in delay, Doppler and phase in order to fully decode the

navigation message. The ‘Block Adjustment of Synchronising Signal (BASS)’ algorithm for Doppler extraction was used. This algorithm is used in software GPS receivers and is comprehensively discussed in [6]. For delay tracking and algorithm based on conventional delayed-locked loop was used [6]. Here we only present the experiment results.

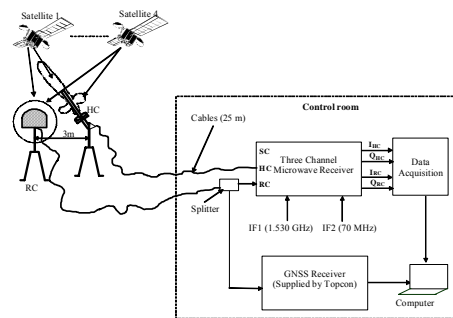


Figure 5: Experimental set-up for synchronisation

Figure 5 shows the experimental set-up for collecting data from the satellite to verify the range compression and synchronisation algorithms. The signal from the satellite was directly received on two channels (radar and heterodyne channels). This topology corresponds to a target at ‘zero range’.

Figure 6 represents the correlation obtained from the proposed range compression algorithm shown in Figure 4. It is seen that the algorithm gives a good correlation and confirms our computer modelling result. As expected, the width (first null) of the main lobe is 0.2μsec and the RMS sidelobe level of -60dB for 45 seconds integration time.

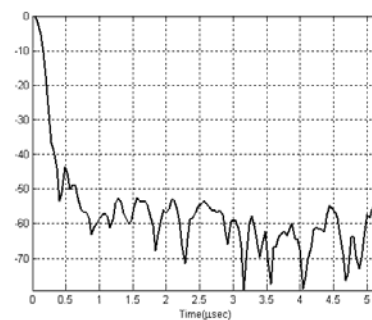


Figure 6: Output of range compression algorithm

Heterodyne Channel Doppler Compensation

Figure 7 shows the experimental set-ups used to verify the imaging algorithm (discussed in the next section). The first set-up consisted of stationary heterodyne channel and moving radar channel (for antenna synthesis). The second experiment represents a more practical scenario where both the heterodyne and radar antennas are moving. It is obvious that the only difference between the two set-ups is the presence of extra Doppler shift in the moving heterodyne channel. This Doppler shift can be large enough to introduce a complete mismatch between the heterodyne channel and the radar channel. Hence one needs to compensate the relative motion between transmitter and receiver.

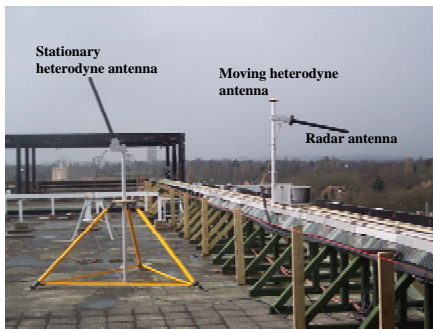


Figure 7: Image experimental set-ups

First of all we consider an instantaneous bistatic triangle formed by the stationary heterodyne channel, shown in Figure 8. The three arms of the bistatic triangle are transmitter-to-receiver path B , transmitter-to-target path R_T and target-to-receiver R_R . For our experimentation with flight imitator we considered targets at short ranges (maximum target range 600m). The typical transmitter-to-receiver range for GLONASS is ~ 20000 km. Therefore the angular separation θ_{Tr} between the transmitter-to-receiver path B and transmitter-to-target path R_T is negligible. Hence for a stationary heterodyne channel, the Doppler shifts due to satellite motion (F_s) in the two paths are similar. The residual Doppler variation after range

compression is present only due to receiver motion relative to target at R_R . This residual Doppler variation in the radar channel forms the azimuth signature of a target. In the imaging algorithm, an appropriate azimuth compression filter is designed for each range bin accordingly. In a practical scenario the heterodyne channel will be in motion as it is mounted on a real aircraft. Figure 8 also shows the bistatic triangle for moving heterodyne channel. The only difference compared to the stationary case is the additional presence of Doppler variation (F_{RS}) due to receiver motion relative to the satellite in the heterodyne channel. It is clear from the figure that the residual Doppler variation is $F_{RS} + F_R$. The question whether F_{RS} can be ignored when designing the azimuth filter is discussed below.

For 20 seconds integration time the maximum tolerable frequency difference between the designed azimuth signature and the actual received signal is $\sim 0.003\text{Hz}^*$. The value of F_{RS} can range from 10-100Hz for an aircraft moving with a velocity of 30m/s. Hence F_{RS} should be estimated and incorporated in the azimuth filter. It should be noted that this problem is not faced in a monostatic SAR as the transmitter and receiver are co-located. The method we used to estimate F_{RS} is explained in the following section with the aid of an experimental setup.

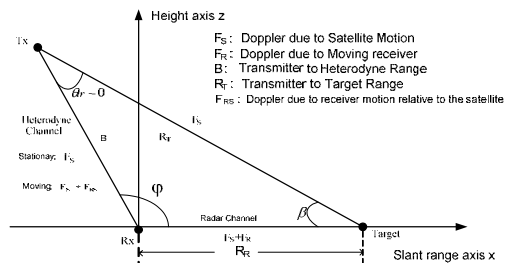
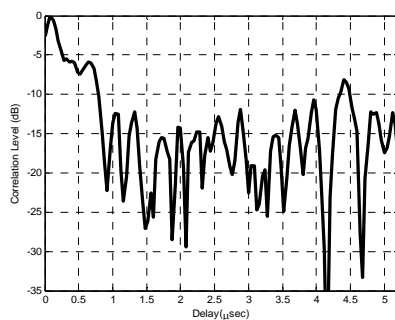


Figure 8: Bistatic triangle for stationary and moving heterodyne

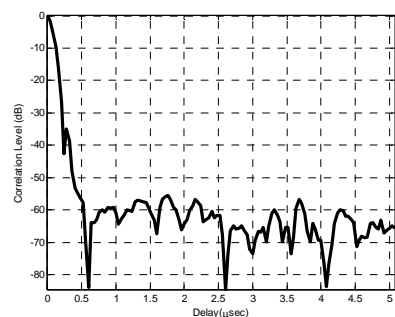
Considering $\pi/8$ phase difference over the integration time

Figure 7 also shows the experimental set-up for collecting data from the satellite to estimate F_{RS} and to verify the moving heterodyne synchronisation. The signal from the satellite was directly received on two channels (moving and stationary). The moving channel antenna was an Omni directional antenna and was separated by some 3m from the stationary channel antenna. The moving channel corresponds to a moving heterodyne channel and we assume the stationary antenna to be a target at ‘zero range’. In this experiment we are ignoring the radar channel as the sole aim of the experimentation is to verify whether we can correctly estimate the F_{RS} .

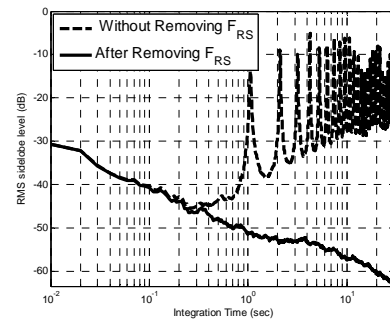
An algorithm was developed that extracts the satellite and the moving antenna positions from the stored data. From this information we calculated the F_{RS} , i.e. Doppler variation due to receiver motion relative to the satellite.



(a)



(b)



(c)

Figure 9: (a) Correlation without removing F_{RS} , (b) Correlation after removing F_{RS} and (c) RMS sidelobe level versus integration time (log scale).

To test that whether we have correctly estimated the F_{RS} , first of all we correlated the moving and the stationary channel without compensating F_{RS} from the moving channel. Due to presence of Doppler difference (F_{RS}) between the two channels, one can expect degradation of correlation function and rise in sidelobe level. Figure 9(a) shows the degradation of correlation function and Figure 9(c) shows a rise in the sidelobe level (dotted line). Figure 9(b) shows the correlations of the two channels after we have removed the F_{RS} from the moving channel. It is seen that after removing the residual Doppler we obtain a good correlation function. As expected, the width (first null) of the main lobe is $0.2\mu\text{sec}$ and the RMS sidelobe level of -64dB for 35 seconds integration time (Figure 9(c)). Hence our estimate of F_{RS} is correct.

SS-BSAR Imaging

Our research has been focused on the derivation of a generalised image formation algorithm designed specifically for SS-BSAR operating in Stripmap mode. In other words, the algorithm exploits the asymmetric geometry of the system for imaging. By the term ‘‘generalised’’, an algorithm able to process data collected with the transmitter and receiver flying in non-parallel flight paths, with unequal velocities is implied. In this section, a conceptual description of the algorithm will be provided. A specific configuration is

assumed, where the transmitter is a GNSS satellite and the receiver is airborne. A full description of the algorithm can be found in [7], [8], along with detailed descriptions of algorithms designed for other SS-BSAR configurations.

A block diagram of the generalised SS-BSAR image formation algorithm is shown in Figure 10. It may be noticed that it is a modification of the standard Range-Doppler algorithm, widely used in monostatic SAR image formation, and thoroughly described in [9].

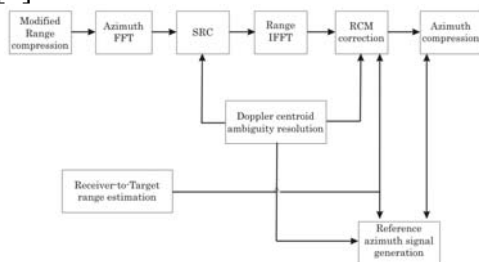


Figure 10: Block diagram of SS-BSAR image formation algorithm

The first step in the algorithm is to equalize the range and Doppler histories of targets residing at the same range from the receiver. This is achieved by applying a single correction function to the SS-BSAR data, which removes the time delay and associated phase due to the transmitter-to-receiver range at each azimuth-time instant. The correction function is integrated with the range compression step; hence the term “modified range compression”. The modified range compression is performed in the range-frequency, azimuth-time domain. At the output of this step, the range and Doppler histories of targets at the same range, but different cross-range become very similar for a wide range of possible geometries. Since the transmitter-to-target and receiver-to-target ranges can normally be approximated using second-order Taylor series expansions in SS-BSAR, it is also possible to derive signal expressions in the frequency domain. Therefore, use of a modification of the Range-Doppler algorithm is a convenient method to form the image of an observation area. A

secondary range compression (SRC) is performed in the two-dimensional frequency domain to compensate for the cross-coupling between the range and azimuth frequencies. Before this operation is executed, the Doppler ambiguity is resolved (that is because the target azimuth signature could contain a large Doppler centroid outside the range of sampled azimuth frequencies). Range cell migration (RCM) is corrected in the range-time, azimuth-frequency (or range, Doppler) domain, after RCM components due to the receiver motion and residual RCM after the modified range compression are calculated. For this operation, it is proposed to estimate the receiver-to-target range from the range sum (the difference between the total range history and the transmitter-to-receiver range history) in order to identify the individual RCM components mentioned above. Finally, azimuth compression is performed in the range, Doppler domain.

Experimental Results

In this section we present one SS-BSAR image obtained by applying the proposed algorithm on experimental data collected from the experimental set-ups shown in Figure 7. Figure 11 shows the SS-BSAR image obtained for moving heterodyne channel (38° bistatic angle). The image obtained from the observation area is superimposed on a satellite photograph of the area. The color-scale is in dB, where 0 dB represents the highest processed echo intensity. It is important to note that the heterodyne channel was moving, therefore, all the algorithms described in previous sections (synchronisation, motion compensation and imaging) were applied to the acquired data. Strong reflections at the near field are observed. Also targets at the range of 240m, 350m, and 500m are visible in the image. Right bottom zoom image shows the strong reflections from the building at 240m.

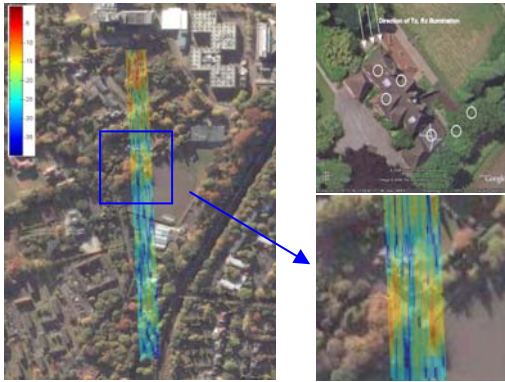


Figure 11: SS-BSAR image for Moving Heterodyne

Figure 12 shows cross-sections of the building shown in Figure 11, taken along the azimuth direction for the image.

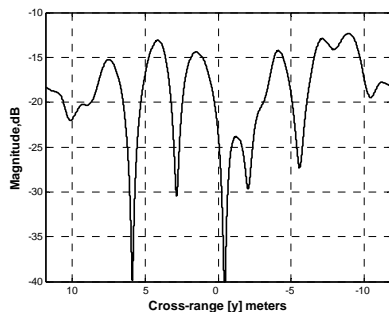


Figure 12: Azimuth cross-sections

Conclusions

This paper gave an overview of the research carried out by the University of Birmingham in the area of SS-BSAR, utilising microwave emissions from GNSS transmitters as the ranging signal. GLONASS satellite was used for experimentation.

It was highlighted that GALILEO and the new GPS satellite are the most prospective candidate for SS-BSAR. Some of the practical problems (such as synchronisation) were also briefly discussed. One of the important problems was moving heterodyne channel. It was discussed that the motion of the heterodyne channel introduces a Doppler shift. This Doppler shift needs to be estimated and incorporated in the azimuth compression filter design. A method to estimate this Doppler shift was described and experimentally verified.

An imaging algorithm for SS-BSAR was briefly discussed and experimentally tested. Using the flight imitator, bistatic images were successfully obtained for moving and stationary heterodyne channel. The next stage of our work will concentrate on obtaining image using a real aircraft.

Acknowledgements

The work reported in this paper was funded by the Electro-Magnetic Remote Sensing (EMRS) Defence Technology Centre, established by the UK Ministry of Defence and run by a consortium of SELEX Galileo, Thales UK, Roke Manor Research and Filtronic.

References

1. Dubois-Fernandez P. et al., "ONERA-DLR bistatic SAR campaign: planning, data acquisition, and first analysis of bistatic scattering behaviour of natural and urban targets", *IEE Proceedings in Radar, Sonar and Navigation*, 2006, 153, pp.214- 223.
2. Walterscheid I. et al., "Bistatic SAR processing and experiments", *IEEE Transactions on Geoscience and Remote Sensing*, 2006, 153, pp.2710-2717.
3. Moccia A. et al., "Spaced-borne bistatic synthetic aperture radar for remote sensing applications", *International Journal of Remote Sensing*, 2000, 21(18), pp.3395-3414.
4. Cherniakov M., Saini R., Antoniou M., Zuo R., Edwards J., "SS-BSAR with transmitter of opportunity - Practical aspects", *3rd EMRS DTC Technical Conference*, 2006, Edinburgh.
5. He, X., Cherniakov, M., Zeng, T., "Signal detectability in SS-BSAR with GNSS non-cooperative transmitters", *IEE Proceedings Radar, Sonar and Navigation*, 2005, 152(3), pp.124-132.
6. Tsui J.B., "Fundamentals of global positioning system receiver - A software approach", *John Wiley & Sons Inc*, 2000.

7. Cherniakov M., Saini R., Zuo R., Antoniou M., “Space-Surface bistatic synthetic aperture radar with global navigation satellite system transmitter of opportunity – experimental results”, *IET Radar, Sonar and Navigation (RSN)*, Vol. 1, issue 6, pp. 447-458, December, 2007..
8. Antoniou M., Cherniakov M., Hu C., “Space-Surface BSAR image formation algorithms”, *IEEE Transactions in Geoscience and Remote Sensing (TGRS)*, under review.
9. Cumming I.G. and Wong F.H., “Digital processing of Synthetic Aperture Radar data”, *Artech House*, Norwood, MA, 2005.